Journal of Palaeogeography, 2025, 14(1): 126–140 (00374)

Available online at www.sciencedirect.com

ScienceDirect

journal homepage: http://www.journals.elsevier.com/journal-of-palaeogeography/

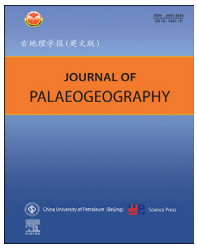

Research article

Autocyclic switching processes and architecture of lobes in river-dominated lacustrine deltas

Zhen-Hua Xu [a,b,*], *Sheng-He Wu* [a,b], *Piret Plink-Björklund* [c], *Tao Zhang* [d], *Da-Li Yue* [a,b], *Qi-Hao Qian* [e], *Qing Li* [a,b], *Wen-Jie Feng* [f]

[a] *National Key Laboratory of Petroleum Resources and Engineering, China University of Petroleum (Beijing), Beijing 102249, China*
[b] *College of Geosciences, China University of Petroleum (Beijing), Beijing 102249, China*
[c] *Department of Geology and Geological Engineering, Colorado School of Mines, Golden 80401, USA*
[d] *Gas Production Plant 2, PetroChina Changqing Oilfield Company, Yulin 719000, Shaanxi Province, China*
[e] *PetroChina Research Institute of Petroleum Exploration and Development, Beijing 100083, China*
[f] *College of Geosciences, Yangtze University, Wuhan 430100, Hubei Province, China*

Abstract River-dominated lacustrine deltas typically consist of multiple lobes due to autogenic lobe switching that occurs over short time scales. However, the switching patterns of multiple lobes in these deltas remain poorly understood, and the architectural features attributed to lobe switching are also lacking. By integrating Delft3D simulations, flume experiments, and modern deposit analysis, we proposed that autogenic lobe switching follows a cyclic pattern. Autocyclicity begins with the formation of an offshore lobe and concludes after a series of longshore lobe growth events, marked by longshore avulsions occurring along the sides of offshore distributary channels. Longshore avulsions follow a sequence that usually occurs earlier distally than proximally and subsequently occurs on one longshore side and then on the other side. Each lobe begins with rapid growth, which gradually slows and then stops once a channel avulsion is influenced by the backwater effect that triggers lobe switching. Three signals indicate lobe switching: a decrease in progradation rate, foreset slope steepening coupled with topset slope gentling, and the deposition of mud-dominated sediments. The number of autocyclic events never exceeds seven. The first two autocyclicities contribute to more than 55% of delta length and 70% of delta area. The lobes are separated by 1–6 stages of mud-dominated accretion beds that exhibit a downstream-inclined shape and convex-up or lateral overlapping pattern. This study conducts a coupled growth-geometric assessment to establish an architectural pattern for river-dominated lacustrine deltas. This architectural pattern offers valuable insights into predicting sandy lobe distribution in river-dominated lacustrine delta reservoirs, and the architecture of muddy accretion beds aids in predicting the rule of oil–water movement and distribution of remaining oil.

Keywords Autocyclic lobe switching, River-dominated lacustrine delta, Architecture, Avulsion sequence, Backwater effect

* Corresponding author. National Key Laboratory of Petroleum Resources and Engineering, China University of Petroleum (Beijing), Beijing 102249, China.
E-mail address: xuzhenhua1003@126.com (Z.-H. Xu).
Peer review under responsibility of China University of Petroleum (Beijing).
https://doi.org/10.1016/j.jop.2024.12.004

Received 9 January 2024; revised 29 May 2024; accepted 16 December 2024; available online 16 December 2024

1. Introduction

The development of river-dominated lacustrine deltas over timescales of decades to millennia is characterized by a sequence of lobe switching. This process involves a primary distributary channel prograding basinward and building a lobe until an avulsion occurs, causing the channel to realign and a new lobe to form (Frazier, 1967). These deltaic sands, which often appear sheet-like and thick, typically have numerous stacked lobes (Yin *et al.*, 2014). The sequence of lobe switching is crucial in determining the delta's stacking pattern and architecture, which are significant for predicting the distribution of hydrocarbon reservoirs.

Two types of processes govern lobe switching: autogenic and allogenic processes (Beerbower, 1964; Holbrook *et al.*, 2003). Allogenic processes control long-term (more than thousands of years) lobe growth and stacking and are influenced by varying supplies, subsidence, and lake level; in contrast, autogenic processes affect lobe switching on short time scales (tens to thousands of years) and over short distances (several to tens of kilometers), because external environmental changes are commonly (although not always) weak and gradual (Holbrook *et al.*, 2003; Olariu, 2014; Straub *et al.*, 2015). Prior studies have linked lobe switching to autogenic factors such as channel incision, avulsion, and lobe abandonment (Muto and Steel, 2004; Martin *et al.*, 2009; Nijhuis *et al.*, 2015; Liang *et al.*, 2016; Hajek and Straub, 2017). However, the switching patterns of multiple lobes in these deltas remain poorly understood, and the architecture attributed to the lobe switching is also missing.

We find that autogenic lobe switching is cyclic (recurrent, though nonperiodic) in river-dominated lacustrine deltas with stable lake levels and ignorable waves/tides. This autocyclic lobe switching can significantly affect the architectural patterns of lobes. Based on observations from modern, experimental, and numerical deltas, our study concentrates on three key aspects of autocyclic switching processes: 1) the patterns of autocyclic lobe switching; 2) the mechanisms underlying autocyclic lobe switching; 3) the architectural patterns of lobes influenced by these switching processes.

2. Datasets and measurements

Flume experiments and Delft3D simulations provide detailed records of delta growth processes and morphological changes (e.g., Edmonds and Slingerland, 2007; Burpee *et al.*, 2015). This paper integrates data from experimental deltas and numerical deltas to analyze autocyclic lobe growth and switching in river-dominated deltas combined with observations from modern river-dominated lacustrine deltas.

2.1. Datasets

2.1.1. Modern river-dominated lacustrine deltas

Historical high-definition satellite images from recent decades document the changes in the southern Mamawi Lake Delta and the southern Aral Sea Delta. In recent decades, these deltas have been river-dominated, experiencing relatively stable lake levels, without influence from tidal or wave processes or human interference. They consist of multiple lobes as illustrated in Fig. 1. Our analysis suggests that lobe switching in these deltas was primarily controlled by autogenic processes, although weak allogenic processes such as fluctuations in lake level and water discharge also played a role.

2.1.2. Experimental deltas

We chose two experimental deltas in this study (Fig. 2). The first experimental delta (EXP1) was built by the SAFL Delta Basin facility (data are from Martin *et al.* (2009) and Wolinsky *et al.* (2010)). The water discharge was set at 0.1 l/s, and the sediment discharge at 1.7×10^{-4} l/s. The bottom slope was ~3 cm/m, and the water depth of the standing body was 30 cm. The detailed experimental setup and procedure were described by Martin *et al.* (2009). The delta formed over 100 h, resulting in the formation of a river-dominated delta (Fig. 2A).

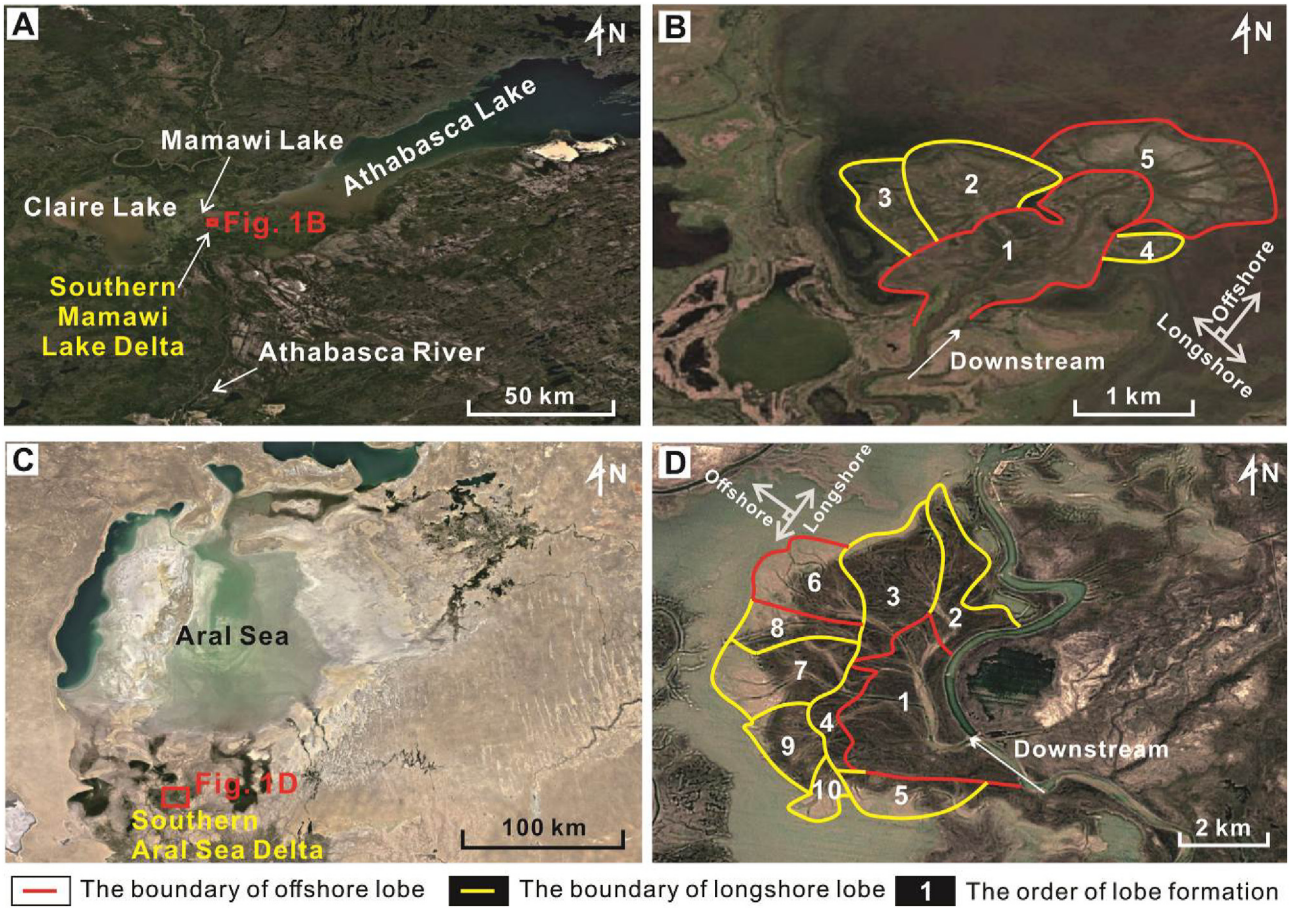

Fig. 1 Satellite maps of modern river-dominated lacustrine deltas. **A)** Location of the southern Mamawi Lake Delta; **B)** Lobe growth history of the southern Mamawi Lake Delta; **C)** Location of the southern Aral Sea Delta; **D)** Lobe growth history in the southern Aral Sea Delta. The southern Mamawi Lake Delta and the southern Aral Sea Delta consist of multiple offshore and longshore lobes.

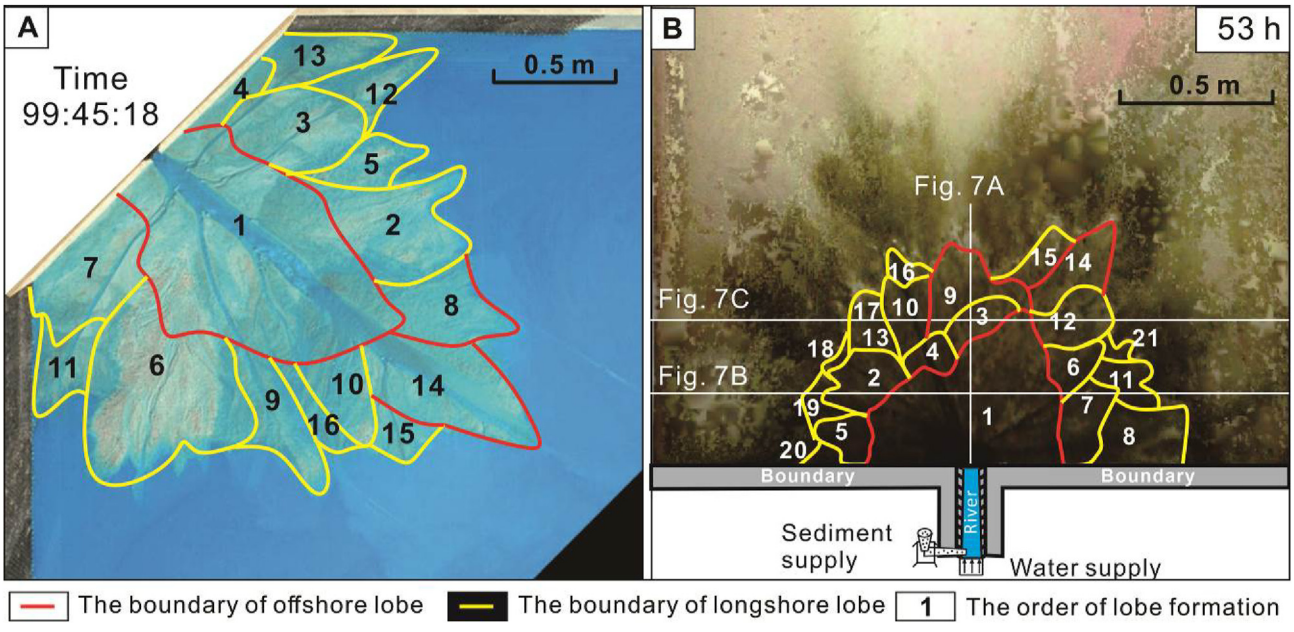

Fig. 2 Map views of lobes in two experimental river-dominated deltas. **A)** EXP1, created by the SAFL Delta Basin facility (Martin *et al.*, 2009; Wolinsky *et al.*, 2010); **B)** EXP2, conducted in the Flume Experiment Laboratory of Yangtze University in China. Both deltas consist of multiple offshore and longshore lobes.

The second experiment (EXP2) was conducted in the Flume Experiment Laboratory of Yangtze University in China (Fig. 2B). The setup consisted of a rectangular region measuring 2.5 m in length and width, and 0.5 m in height, with a uniformly gentle slope of 0.5 cm/m. To maintain a constant water depth of 3 cm in the river mouth, the water level was kept steady. The initial river bed, measuring 0.3 m in length and 0.05 m in width, was positioned in the southern region. The river had a depth of 3 cm with a flat bottom. A water pump supplied water into the river, maintaining a discharge of 0.3 l/s. A sediment supplying mechanism carried sediments into the river, keeping the sediment discharge at 1.0×10^{-4} l/s. The sediments mixed with the water in the river, resulting in a sediment concentration of ~0.8 kg/m3. The sediments used in the experiment were artificial silica sands and bentonite clays. The grain size ranged from 10 μm to 500 μm and followed a normal distribution, with a median size (D50) of approximately 100 μm and a sand/mud ratio of 0.4. To enhance the mixture's cohesiveness and promote the development and maintenance of stable channels, a small amount (0.2%) of a commercially available polymer was added (Martin *et al.*, 2009). The flume experiment, which ran for 53 h, resulted in the formation of a river-dominated delta. We documented the depositional process through video recordings and conducted hourly scans of the landform using a laser scanner, as shown in Fig. 2B.

The above two flume experiments maintained a constant water level, stable topography, and a relativity steady supply of water and sediment. The sediment mixtures remained consistent in composition throughout the experiments. Consequently, the development of these two deltas was driven by autogenic processes, unaffected by external changes.

2.1.3. Numerical deltas

Delft3D (version 4.01.01) is an effective tool for simulating river-dominated deltas, as evidenced by prior studies (Edmonds and Slingerland, 2007; Burpee *et al.*, 2015). A physics-based morphodynamic model was constructed using a numerical fluid-flow and sediment transport model. The model treats flow as incompressible and with a free surface, computed by solving the depth-integrated, Reynolds-averaged Navier—Stokes equations (Caldwell and Edmonds, 2014). Morphological changes were updated using the Exner equation for sediment mass conservation (Wang *et al.*, 2016). We selected the transport formula from Van Rijn (1993) to differentiate between suspended and bedload transport. Fine sediments (diameter ≤64 μm) were considered cohesive sediments that were transported in suspension, and their settling velocities were transformed by Stokes' law, neglecting flocculation. Coarse sediments (diameter >64 μm) were considered noncohesive sediments that were transported as suspended load and bedload, and their settling velocities were calculated by the method from Van Rijn (1993). Bedload transport direction was adjusted according to local flow conditions and bed-slope effects. We chose the predictor from Van Rijn (1993) and parameterizations of transverse slopes from Ikeda (1982) to calculate the bed-slope effects to counteract high incisions (Baar *et al.*, 2019).

The simulation domains mirrored the scales of modern river-dominated deltas, measuring 10 km by 8 km with a 40 m by 40 m cell size. Five simulations (SIM0—SIM4) were carried out with a moderate cohesive sediment mixture and negligible wave and tidal processes. SIM0 was used as a reference simulation. Compared to SIM0, the other four simulations were carried out with different initial water depths at the river mouth (SIM1), initial basin slopes (SIM2), discharges (SIM3), and lake levels (SIM4). The morphological scale factor of 175 was employed to accelerate the rate of morphological changes (Burpee *et al.*, 2015). Numerical deltas evolved over thousands of simulated hours, corresponding to hundreds of years of natural changes. The specific simulation parameters are detailed in Table 1. Plan views and successive lobe growth are depicted in Fig. 3.

SIM0—SIM2 were subject to autogenic processes, as the depositional conditions remained constant. In contrast, SIM3 and SIM4 not only experienced autogenic processes but also encountered short-term allogenic processes, such as fluctuations in water discharge and lake levels.

2.2. Metric measurements

To quantify the lobe-switching processes, we identified lobes in the deltas. To assess the architecture, we focused on metrics concerning the dimension and stratigraphic architecture of the deltas. The definitions and methods for measuring these metrics are outlined as follows:

1) Lobes. Lobe switching was identified from the avulsions of distributary channels (Beerbower, 1964; Cecil, 2003). River-dominated lacustrine deltas in Figs. 1—3 consist of multiple lobes, recognized by distributary channel avulsions. The lobes can be divided into offshore and longshore types based on the progradation directions of distributary channels (Figs. 1—3). For offshore lobes,

Table 1 Simulated parameters of the Delft3D simulations.

Simulated parameters	SIM0	SIM1	SIM2	SIM3	SIM4
Initial water depth of the river mouth (m)	2	4	2	2	2
Initial basin slope (°)	0.046	0.046	0.099	0.046	0.046
Discharge (m^3/s)	1200	1200	1200	1000—1400	1200
Lake level (m)	0	0	0	0	−0.25—0.25
Initial channel dimensions (length × width × depth) (m^3)	480 × 280 × 2.5				
Highland dimensions (length × width × elevation) (m^3)	10000 × 500 × (−1)				
Grain size of sediment factions (μm)	300, 150, 80, 32, 13, 7.5				
Corresponding proportions of sediment fractions (%)	10, 10, 20, 30, 20, 10				
Initial sediment layer thickness at the bed (m)	10				
Total sedimentary concentration within the river (kg/m^3)	0.1				
Cohesive sediment critical shear stress for erosion (N/m^2)	0.5				
Time step (min)	0.2				
Morphological scale factor	175				
Chézy value for hydrodynamic roughness (m^2/s)	45				
Spin-up interval before morphological updating begins (min)	1440				
Factor for the erosion of adjacent dry cells	0.25				

the distributary channels mainly prograde lakeward, and the lobes primarily contribute to the delta length. In contrast, for longshore lobes, the distributary channels prograde both lakeward and along the shore, and commonly mainly along the shore at the sides of offshore lobes. The longshore lobes mainly contributed to the delta width, and could not increase delta length.

2) Dimension. We considered the length, width, and area to characterize the delta dimension. The delta length and width were quantified by the maximum offshore and longshore progradation distances. The delta area was measured according to the distribution of the subaerial area (excluding the distributary channel). The wetted area—land area maps that partition each image into subaqueous vs. subaerial pixels were created to help calculate the delta area (subaerial area). In addition, we measured the rate of delta area increase, which was defined as the difference in the delta area between two defined time periods (every four simulated hours).
3) Stratigraphic architecture. To quantify the stratigraphic architecture, we used the stratigraphic progradation rate, slope, and sediment grain size. The stratigraphic progradation rate was defined as the difference in the foreset progradation distance across two defined time periods (every four simulated hours) in the progradation direction. We measured the foreset and topset slopes by calculating the average slope at each end of the foreset and topset, respectively. The foreset thickness was determined by the height difference at the two ends of the foreset. Sediment grain size was quantified using the median diameter, D50.

Some of the above metrics were normalized to adjust values at different scales to a notionally common scale, where the maximum normalized value was equal to 1.

3. Results

3.1. *Autocyclic lobe switching processes*

3.1.1. Autocyclic lobe switching processes without any allogenic process

River-dominated lacustrine deltas depicted in Fig. 1B—D, 2A, B, and 3A—C, typically consisted of multiple lobes. A few of these (23% in average) were offshore lobes, which occupied the central axis of the delta, while the majority (78% in average) were longshore lobes that covered most of the delta area (mostly >60%) and encircled the offshore lobes.

The formation of these lobes followed a similar cycle: An offshore lobe initially formed at the center, followed by the sequential formation of longshore lobes. We defined the autocyclicity of lobe switching to include the initial switching of an offshore lobe and subsequent switching among longshore lobes. Each cycle, therefore, started with the growth of an offshore lobe and concluded just before the last longshore lobe switched. Longshore lobe switching typically alternates from distal to proximal positions and from one side of the delta to the other until the accommodation space is filled. For instance, in SIM0 (Fig. 3A), after the formation of the offshore lobe (lobe 1) in the central area, three longshore lobes (lobes

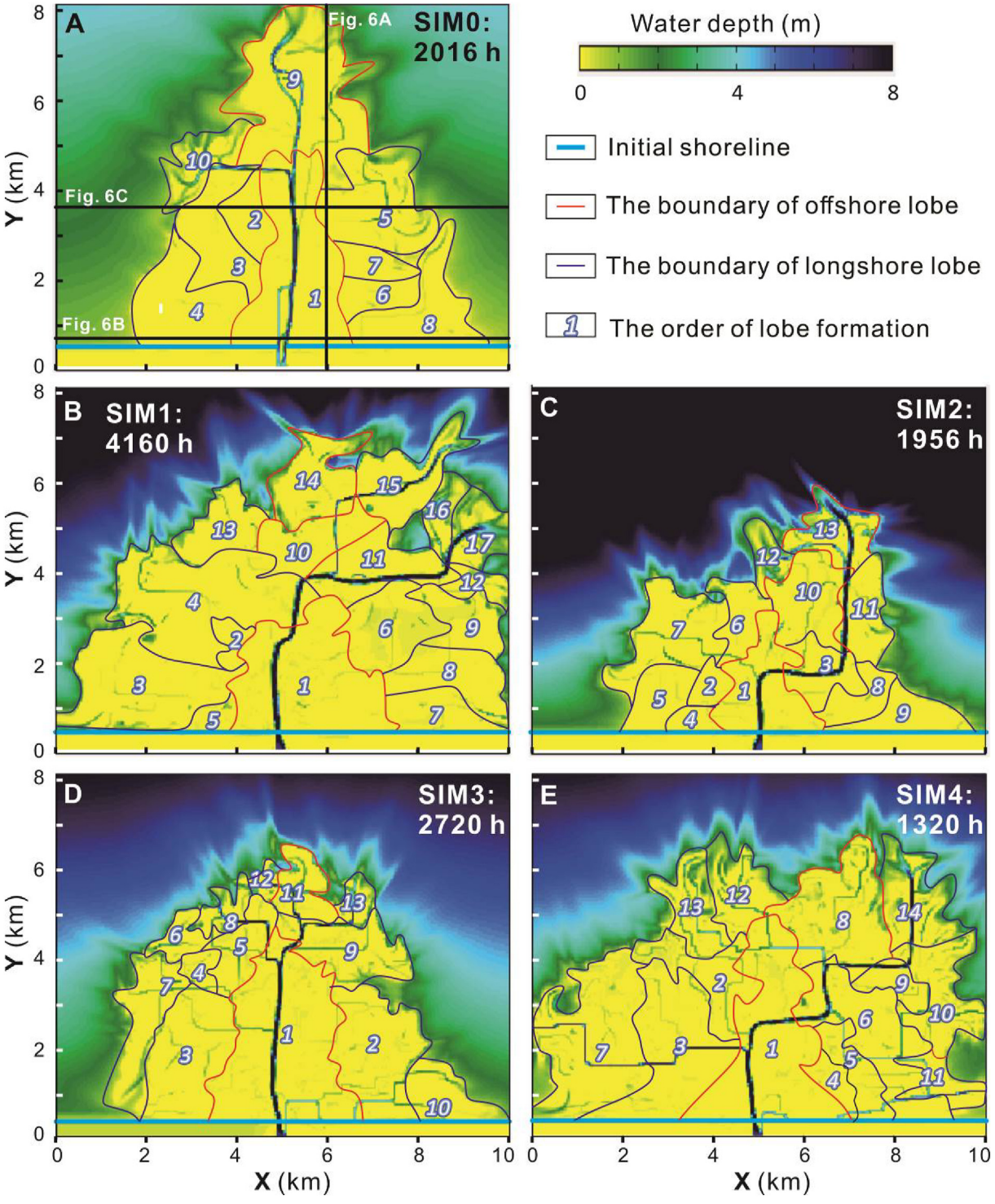

Fig. 3 Map views of five simulated river-dominated deltas: SIM0 (A), SIM1 (B), SIM2 (C), SIM3 (D), and SIM4 (E). The depositional environmental differences encompass variations in basinal water depth and slope. The numbers indicate the order of lobe formation.

2—4) were deposited on the left side of the offshore lobe, from distal to proximal positions. The accommodation space on the left side was filled. Subsequently, four longshore lobes (lobes 5—8) were deposited on the right side of the offshore lobe, also from distal to proximal positions. And the accommodation space on the right side was also filled. A new offshore lobe (lobe 9) then formed at the terminus of lobe 1, and finally, a longshore lobe (lobe 10) was deposited on the left side of the offshore lobe 9.

Fig. 4 shows the changes in progradation rates of lobes in SIM0. It illustrated that each lobe started with rapid progradation (exceeding the average lobe progradation rate) and that progradation gradually slowed and stopped after a new lobe formed, due to the occurrence of channel avulsion. The rapid progradation period was short, but most of the lobe was built during this time. In contrast, the slow progradation period was much longer but contributed less to lobe building. As soon as the slow progradation period started, lobe switching was triggered, and a new lobe began to form through rapid progradation. Thus, slow progradation served as a signal for lobe switching and the rapid progradation of a new lobe.

River-dominated lacustrine deltas could undergo several autocyclicities, as evidenced by the growth of new offshore lobes (Fig. 1B—D, 2A, B, and 3A—C). In each new autocyclicity, lobes were deposited at a far-shore location compared to those in the previous autocyclicity. As a result, river-dominated lacustrine deltas gradually prograded basinwards.

3.1.2. Autocyclic lobe switching processes with short-term allogenic process

Modern river-dominated lacustrine deltas (the southern Mamawi Lake Delta and southern Aral Sea Delta) and numerical deltas (SIM3 and SIM4) primarily experienced autogenic processes, but they were also influenced by weak short-term allogenic processes (such as fluctuations in river discharge and lake level)

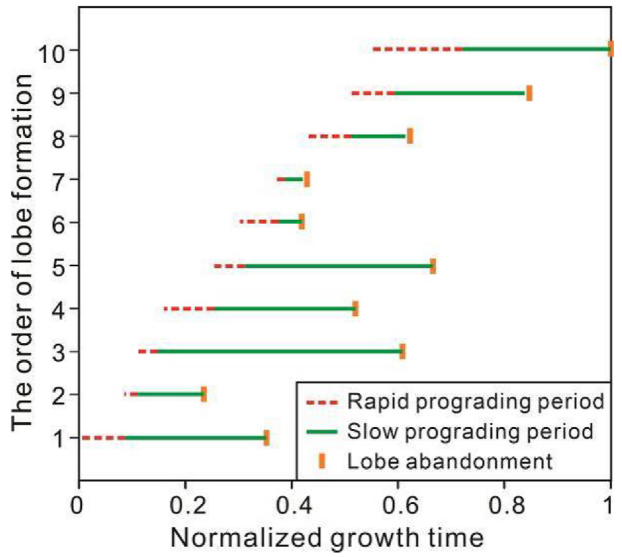

Fig. 4 Changes in the progradation rate of the lobes in SIM0. Lobe growth started with rapid progradation (> average lobe progradation rate), and the progradation gradually slowed and stopped.

(Fig. 1B—D, 3D, E). These deltas continued to exhibit autocyclic lobe switching processes, wherein an offshore lobe initially forms, followed by the formation of a series of longshore lobes at the sides of the offshore lobe. Fluctuations in river discharge and lake level, however, disrupted the sequences of autocyclic lobe growth and switching. Although longshore lobe switching did not strictly follow previous patterns, it tended to alternate from distal to proximal positions and from one side to another (Fig. 1B—D, 3D, E). In each new autocyclicity, lobe switching and growth mostly occurred at far-shore locations compared to those in the previous cycles. Nevertheless, some lobes, such as lobe 10 in SIM3 and lobes 9—11 in SIM4, were still deposited at nearshore locations (Fig. 3D and E).

3.2. Time-varying delta architecture with autocyclic lobe switching

3.2.1. Dimensions

1) Delta length and width

Delta length and width increased with delta growth, but they exhibited alternating rates of increase. Initially, both dimensions increased, driven by the growth of the first offshore lobe. Subsequently, the delta width increased more rapidly than the length due to a series of longshore lobe growths. Following this, the delta length increased rapidly while the delta width barely changed, influenced by the growth of a new offshore lobe in the next autocyclicity. Therefore, these alternating rates of increase were closely linked to autocyclic lobe switching. Multiple autocyclicities had led to intermittent increases in delta length and width as the delta growth progressed (Fig. 5A).

Delta width was mainly controlled by lobe growth during the first autocyclic period, accounting for 70%—90% of the total width (Figs. 1—3). The offshore lobe contributed to a 20%—40% increase in total delta width, while the subsequent sequence of longshore lobe growth substantially increased the delta width by 40%—60%. The proximal longshore lobes made greater contributions to delta width due to their extensive longshore progradation compared to the distal longshore lobes (Figs. 1—3). In subsequent autocyclicities, increases in delta width were limited to only 10%—30% of the total width (Fig. 5A).

The increase in delta length during an autocyclicity decreased with the number of autocyclicities (Fig. 5A). L_n was defined as the ratio of the delta length increase in an autocyclicity to the total delta length, and it exhibited a negative logarithmic relationship with the

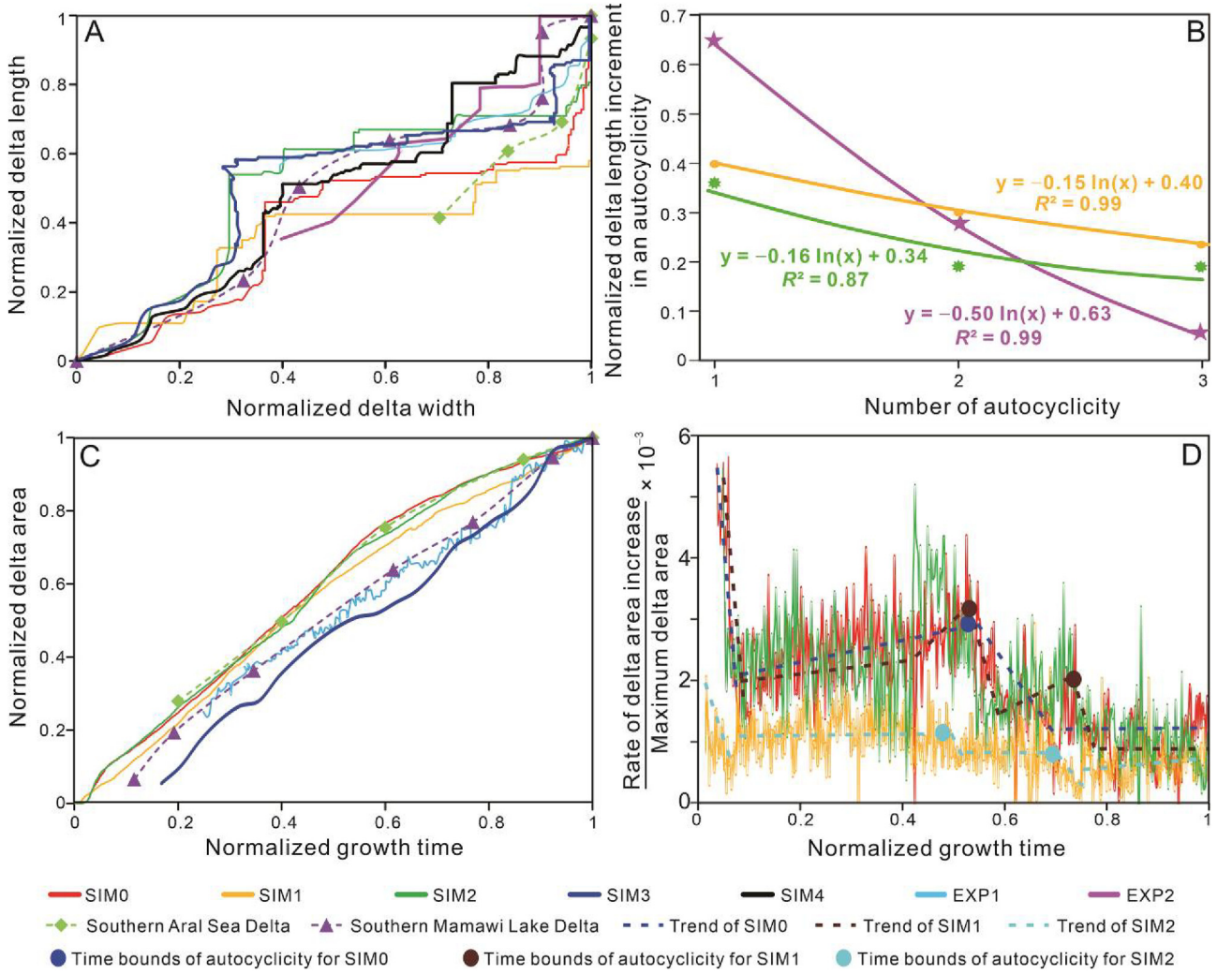

Fig. 5 **A)** Relationships between normalized delta length and width during delta growth; **B)** Normalized delta length increment in an autocyclic process; **C)** Time-varied normalized delta areas; **D)** The rate of delta area increases through time.

number of autocyclicities (Fig. 5B). This relationship can be expressed as follows:

$$L_n = -a \ln(N) + b \quad \text{(Equation 1)}$$

where N was the number of autocyclicity; a was the decrease rate; b was the ratio of the delta length increase in the first autocyclicity to the total delta length.

Based on the nine river-dominated lacustrine deltas in this paper, we calculated b/a values, which were 1—3. L_n was negligible after the 7th autocyclicity. The first two autocyclicities made primary contributions to the delta length, which were more than 55% of the total delta length and reached 95% of the total delta length in EXP2.

2) Delta area

Time-series analysis revealed that the delta area increased with increasing delta growth, as illustrated in Fig. 5C. However, the rate of increase in delta area (ΔA) decreased over time for the river-dominated lacustrine deltas as depicted in Fig. 5D. ΔA was characterized as a stepwise decrease within each consecutive autocyclic cycle. During the autocyclic process, ΔA initially decreased over time, corresponding to the offshore lobe growth period. It then fluctuated and exhibited slightly increasing trends during the longshore lobe growth period (Fig. 5D). The first growth cycle mostly accounted for 40% of the final delta area, and the first two growth cycles together accounted for 70% of the final area in the simulated and experimental deltas (Fig. 5A—C). Longshore lobe growth played a significant role in the delta-building process, contributing to more than 60% of the total delta area.

3.2.2. Stratigraphic architecture

The stratigraphy of river-dominated lacustrine deltas was comprised of topset, foreset, and bottomset layers, as demonstrated by the stratigraphic sections of SIM0 and EXP2 (Figs. 6 and 7). The slopes of the topset and foreset, as well as the foreset thickness, experienced complex changes during delta growth. Regardless of whether it was offshore or longshore progradation, rapid progradation tended to increase the foreset slope and thickness while decreasing the topset slope in the progradation direction. Conversely, slow longshore progradation resulted in an increase in the topset slope, and a decrease in the foreset slope and depth. Quantified measurements from EXP2 further revealed these opposite stratigraphic changes between rapid and slow progradation directions, as well as between the topset and foreset slopes within the same progradation direction (Fig. 8). These contrasting changes were associated with the alternating rapid progradation of offshore and longshore lobes.

The topset and bottomset consisted of mud-dominated sediments, while the grain size in the foreset varied with delta growth (Fig. 6). In the foreset, rapid progradation induced the deposition of sand-dominated sediments due to high water-flow velocity, whereas slow progradation led to the deposition of mud-dominated sediments as a result of low water-flow velocity. Consequently, rapid offshore progradation resulted in sand-dominated foresets on the offshore direction and mud-dominated foresets on the longshore direction, and vice versa (Fig. 6).

Lobe growth began with rapid progradation, characterized by sand-dominated deposits with a relatively steep slope, and then transitioned to slow progradation, resulting in mud-dominated deposits with a gentle slope. This transition from steep to gentle slopes in the foreset, which prominently featured mud-dominated sediments, effectively revealed the boundaries of lobes within river-dominated lacustrine deltas, as observed in SIM0 (Fig. 6).

4. Discussion

4.1. Mechanism of autocyclic lobe switching in river-dominated lacustrine deltas

Autocyclic lobe switching of river-dominated lacustrine delta is influenced by autogenic channel avulsions, which induce new lobe formation and old lobe abandonment. Hoyal and Sheets (2009) proposed

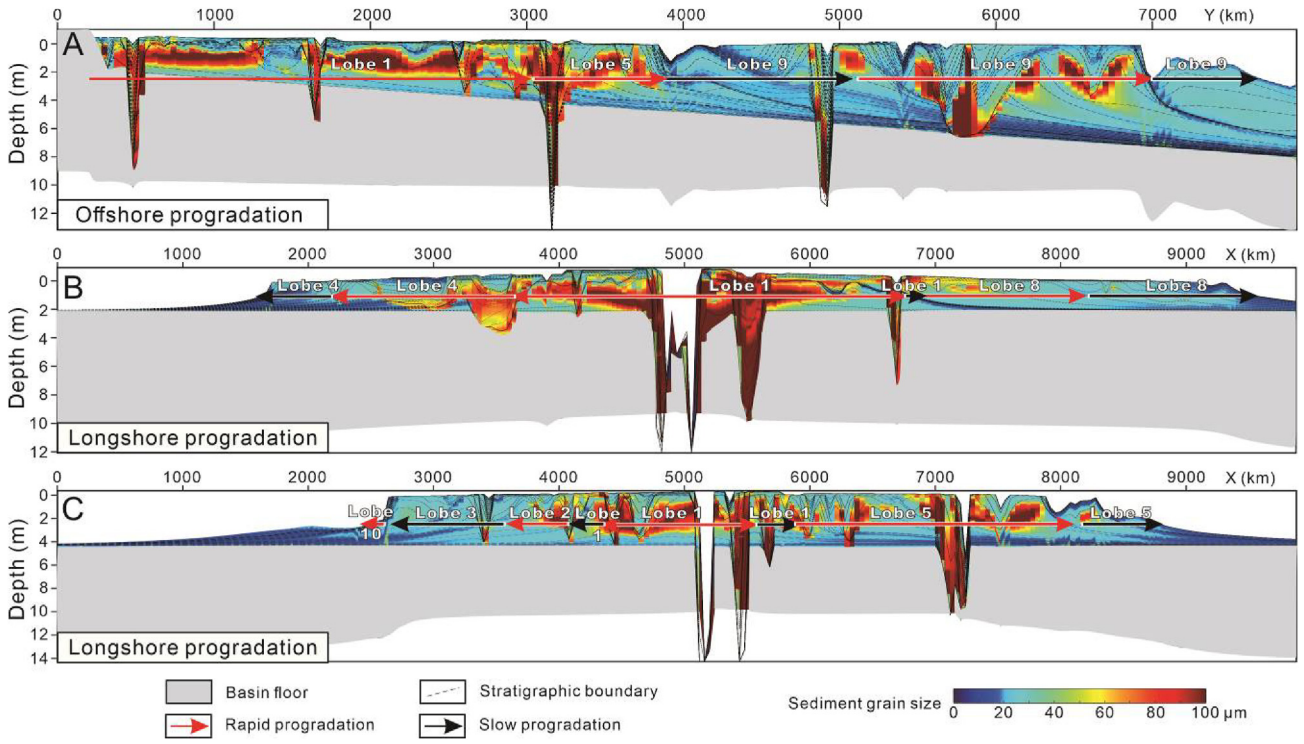

Fig. 6 Stratigraphic sections of SIM0. The locations of the sections are shown in Fig. 3A. Rapid progradation led to an increase in the foreset slope, foreset thickness, and the deposition of sand sediments in the progradation direction, in contrast to slow progradation. Changes in the topset slope were not documented. The topset and bottomset sediments were predominantly mud. Rapid progradation resulted in sand-dominated foresets, whereas slow progradation led to mud-dominated foresets.

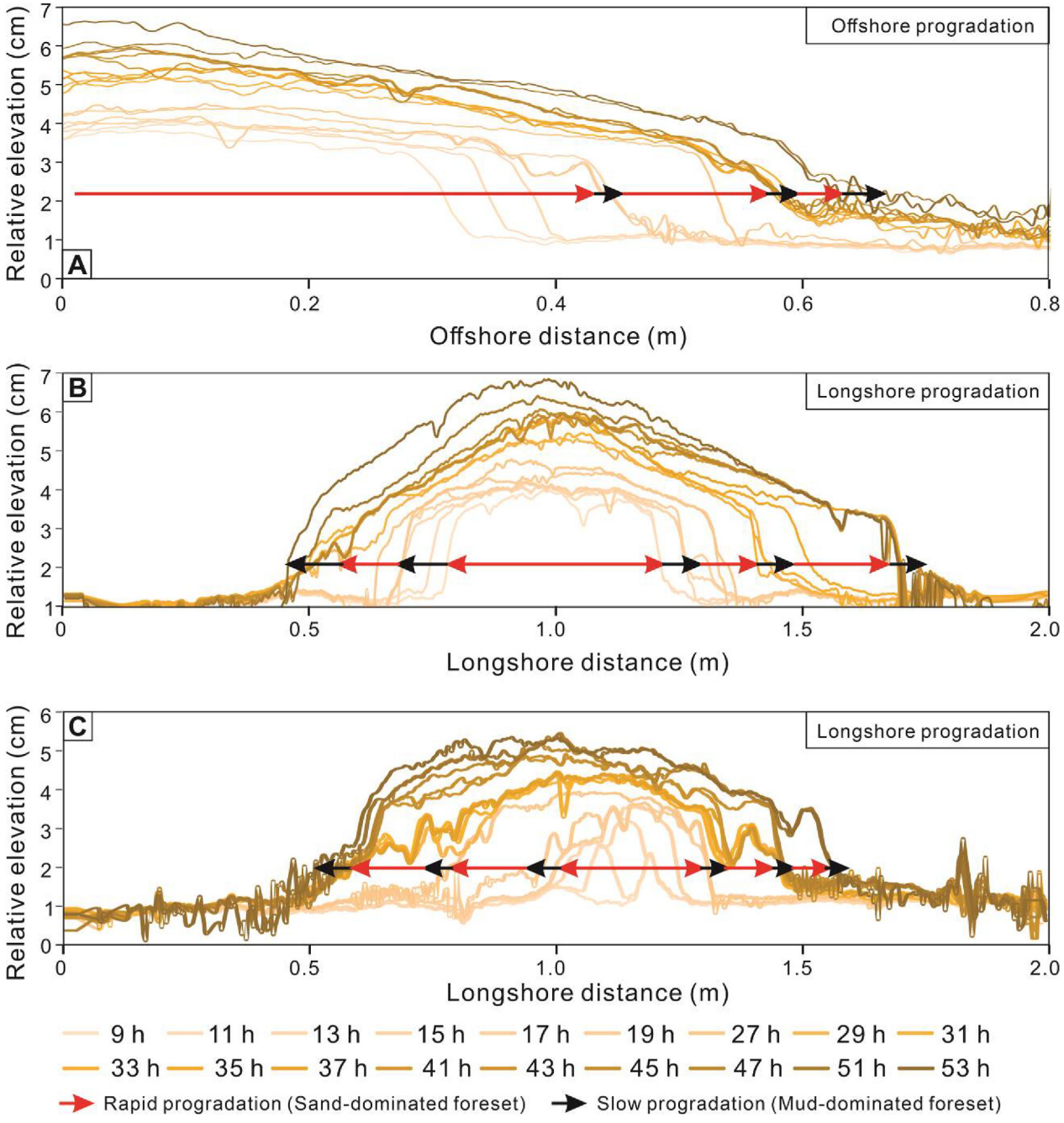

Fig. 7 Stratigraphic sections of EXP2. The locations of the sections are shown in Fig. 2B. Rapid progradation increased the foreset slope and thickness, and deposition of sandy sediments and decreased the topset slope on the progradation direction, opposite to slow progradation.

the 'morphodynamic backwater effect' to explain channel avulsion near the shoreline. According to this theory, bar deposition near the shoreline leads to an upstream migrating flow disturbance. This disturbance causes sedimentation to propagate up the channel and results in channel superelevation, which ultimately leads to overbank flooding and channel avulsion. This theory provides a basis for explaining the autocyclic lobe switching in river-dominated lacustrine deltas.

We find that the backwater effect occurs and that the distributary channel avulses when slow progradation begins (Fig. 4), which can be explained by the change in the stratigraphic architecture. Rapid progradation increases the foreset slope and thickness in the progradation direction. The distributary channel then requires additional time to fill the basinal space in front of the channel outlet, reaching the elevation of the fluvial surface before it can propagate efficiently

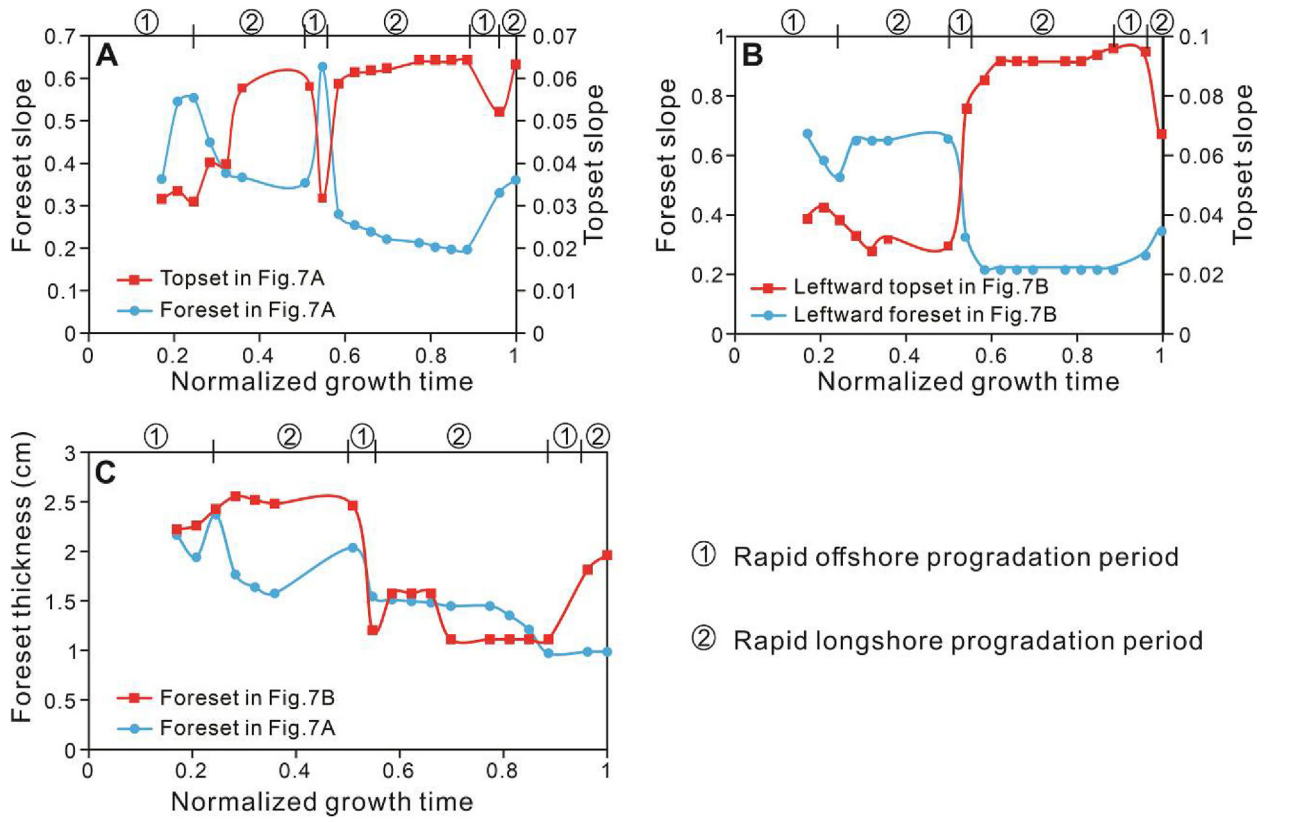

Fig. 8 Changes in the stratigraphic slope and foreset thickness in EXP2. During rapid offshore progradation period, the foreset slope and thickness increased, and the topset slope decreased on the offshore direction; while the foreset slope and thickness decreased, and the topset slope increased on the longshore direction. In contrast, the foreset and topset exhibited opposite changes during rapid longshore progradation period.

(Hoyal and Sheets, 2009). Subsequently, the topset slope becomes gentler, channel flow decelerates, and lobe progradation slows, leading to channel bed aggradation and superelevation (known as the backwater effect). Moodie *et al.* (2019) also proposed that the lobe growth drives upstream channel bed aggradation as lobe progradation extends channel length. Consequently, channel avulsion and lobe switching typically occur on the other side, where the foreset slope and thickness are smaller and the topset slope is higher, facilitated by slow lobe progradation. The direction of avulsion often aligns with the lobe progradation direction, as these represent the shortest paths to the shoreline (Ganti *et al.*, 2016). Thus, a new lobe begins to grow rapidly, while the old lobe grows more slowly and is gradually abandoned. As a result, river-dominated lacustrine deltas exhibit autocyclic lobe switching, characterized by alternating growth between offshore and longshore lobes.

After rapid offshore progradation, the sides of offshore lobe create favorable conditions for channel avulsion, leading to the switching and growth of a series of longshore lobes until the suitable spaces are largely filled (Figs. 1—3). Both numerical and experimental deltas have demonstrated that longshore lobe switching tends to alternate between distal to proximal positions and from one side to the other. This sequence can also be explained by the backwater effect. The cross-levee flow, generated by channel bed aggradation during the backwater period, is a necessary condition for avulsion (Edmonds *et al.*, 2009). Channel bed aggradation, caused by the backwater, migrates upstream from the channel outlet (Hoyal and Sheets, 2009). Consequently, avulsion locations are more likely to shift upstream (Moodie *et al.*, 2019). Moreover, rapid progradation of a longshore lobe on one side of an offshore lobe causes the foreset on this side to become gentler and thinner. Consequently, the new longshore lobe prefers to form on this side.

Short-term allogenic processes triggered by climate changes, human intervention (Ma *et al.*, 2010; Hamilton and Stampone, 2013; Wei *et al.*, 2020), large volcanic eruptions, or the 11-year sunspot cycle (Mishra *et al.*, 2014; Stenchikov, 2021), can cause fluctuations in discharge and lake levels. These

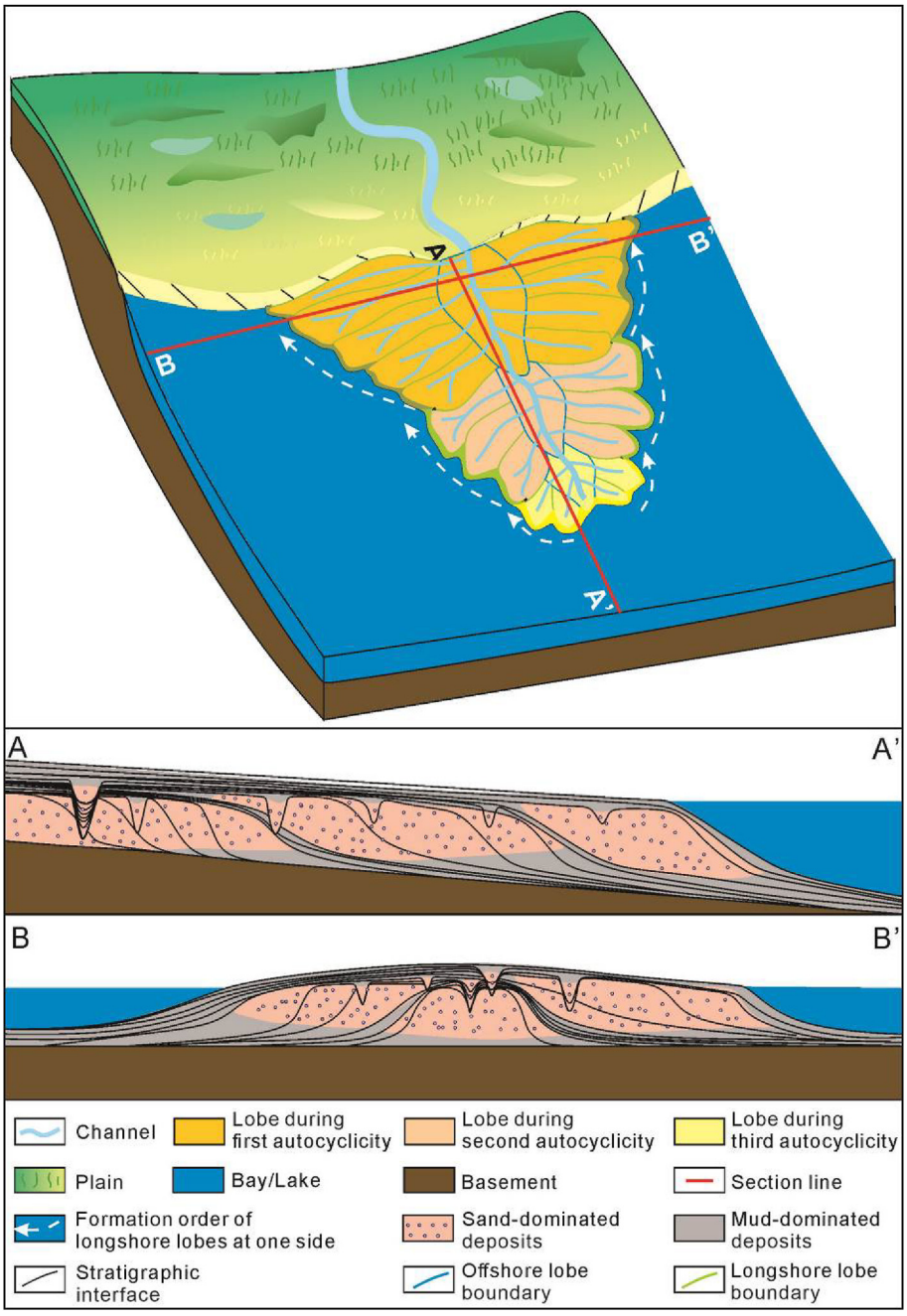

Fig. 9 Architectural pattern of river-dominated deltas attributed to autocyclic lobe switching.

fluctuations may affect avulsion location and frequency (Martin *et al.*, 2009; Ganti *et al.*, 2014), by disturbing processes of channel bed aggradation and superelevation, although do not impact the avulsion timescale (Moodie *et al.*, 2019; Chadwick *et al.*, 2022). Despite the presence of short-term allogenic processes, river-dominated lacustrine deltas continue to undergo autocyclic lobe switching. However, longshore lobe switching does not strictly adhere to the pattern of alternating from distal to proximal positions and from one side to another.

4.2. Autocyclic lobe switching pattern in river-dominated lacustrine deltas

The lobe never grows beyond a certain size or extends beyond a certain length (Donaldson, 1966; Gao, 2007). As a result, river-dominated lacustrine deltas commonly consist of multiple lobes, such as southern Mamawi Lake Delta and southern Aral Sea Delta. Given the minimal or weak external environmental changes, lobe switching in these deltas is predominantly autocyclic, driven by the autogenic backwater effect.

In an autocyclicity, an offshore lobe initially forms, followed by the formation of a series of longshore lobes, driven by switching from the offshore lobe to multiple longshore lobes. Longshore lobe switching tends to alternate between distal to proximal positions and from one side to the other. In a subsequent autocyclic process, lobes switched are deposited at locations farther shorewards compared to those in the previous autocyclicity.

There are three aspects of lobe switching signals:

1) Lobe progradation slowing. All lobe growth begins with rapid progradation, which gradually slows and stops after a new lobe forms. This slowing of lobe progradation suggests that an avulsion is imminent, marking the end of one lobe's growth and the initiation of another.
2) Foreset slope steepening and topset slope gentling. Rapid progradation results in the steepening of the foreset slope and the gentling of the topset slope in the progradation direction, triggering the backwater effect and channel superelevation, which suggest an impending avulsion.
3) Deposition of mud-dominated sediments. Rapid progradation carries sand-dominated sediments on the foreset, whereas slow progradation carries mud-dominated sediments. The deposition of mud-dominated sediments signals slow progradation and subsequent channel avulsion.

4.3. Lobe architectural pattern attributed to autocyclic lobe switching

The depositional architecture of river-dominated lacustrine deltas has been studied further, especially for distributary channels (e.g., Edmonds and Slingerland, 2007; Fu *et al.*, 2015) and mouth bars (e.g., Yin *et al.*, 2015; Feng *et al.*, 2018; Xu *et al.*, 2023). Research by Yin *et al.* (2015), Feng *et al.* (2018), and Xu *et al.* (2023) suggested that mouth bars develop multiple-stage, mud-dominated accretion beds that take on a downstream-inclined shape in downstream sections and display convex-up (upwarping) or lateral overlapping patterns in longshore sections. The convex-up accretion beds are interpreted as the vertical stacking of mouth bars during periods of base-level fall, while the lateral overlapping patterns indicate the stacking of laterally migrated mouth bars during base-level rise (Yin *et al.*, 2015). Typically, a single-stage delta forms over tens to hundreds of years and is primarily influenced by autogenic processes, though it can be disturbed by allogenic processes.

This paper proposes an architectural pattern for river-dominated lacustrine delta, attributed to autocyclic lobe switching (Fig. 9). The delta is composed of 1—6 autocyclic lobe complexes, each consisting of an offshore lobe and a series of longshore lobes. As the number of autocyclic events increases, the length and area of each lobe decrease. Notably, the first two autocyclic lobe complexes, especially the longshore lobes, contribute to more than 70% of the final delta area. Within a lobe, sandy sediments predominate due to rapid growth, while mud-dominated accretion beds separate the lobes, reflecting slower growth period. The 1—6 stages of accretion beds formed by offshore lobes exhibit a downstream-inclined shape, whereas those formed by longshore lobes display convex-up or lateral overlapping patterns (Fig. 9). With an increase in autocyclicites, the spacing between adjacent downstream-inclined accretion beds diminishes. Typically, a delta comprises fewer than five accretion beds, correlating with the common occurrence of fewer than five autocyclicites. Short-term allogenic processes may disrupt the shape and continuity of these accretion beds. This architectural pattern offers valuable insights into the detailed development of delta reservoirs.

5. Conclusions

This study proposes that lobe switching in river-dominated lacustrine deltas on short time scales follows an autocyclic pattern, triggered by the backwater effect. This autocyclic pattern and resulting lobe architecture are summarized below:

1) Autocyclicity begins with an offshore lobe and concludes after a series of longshore lobe growth events. Longshore lobe switching tends to alternate between distal and proximal positions and from one side to another. Each lobe begins with rapid growth, which gradually slows and then stops after a channel avulsion triggers lobe switching.
2) Three signals indicate lobe switching: a decrease in progradation rate, foreset slope steepening coupled with topset slope gentling, and the deposition of mud-dominated sediments.
3) The number of autocyclic events never exceeds seven. The length and area of lobes decrease as the number of autocyclicities increases. The first two autocyclicities contribute to more than 55% of delta length and 70% of delta area. The lobes are separated by 1—6 stages of mud-dominated accretion beds that exhibit a downstream-inclined shape and convex-up or lateral overlapping pattern.

CRediT authorship contribution statement

Zhen-Hua Xu carried out the numerical simulations and flume experiments, participated in the analysis of autocyclic switching processes and architecture, and drafted the manuscript. Sheng-He Wu and Piret Plink-Björklund conceived of the study, and participated in its design and coordination and helped to draft the manuscript. Tao Zhang and Qi-Hao Qian performed the statistical analysis. Da-Li Yue and Qing Li helped to draft the manuscript. Wen-Jie Feng participated in the analysis of delta architecture and helped to draft the manuscript. All authors read and approved the final manuscript.

Availability of data and material

The simulation and experiment data in this paper are uploaded in the Mendeley data, and can be downloaded at https://doi.org/10.17632/kb7bbdnctv.1.

Funding

This study is supported by the National Natural Science Foundation of China (No. 42202178) and Science Foundation of China University of Petroleum (Beijing) (No. 2462023YJRC034).

Declaration of competing interest

The authors declare that they have no known competing financial interests or personal relationships that could have appeared to influence the study reported in this paper. This manuscript is approved by all authors for publication. None of any part of the content has been published or has been accepted elsewhere. It is also not being submitted to any other journal at the same time.

Acknowledgements

We thank Wolinsky *et al*. for kindly sharing data of the experimental delta. We thank two Associate EiCs (Yuan Wang and Santanu Banerjee) and other anonymous reviewers for constructive reviews that significantly improved the manuscript.

References

Baar, A.W., Boechat Albernaz, M., van Dijk, W.M., Kleinhans, M.G., 2019. Critical dependence of morphodynamic models of fluvial and tidal systems on empirical downslope sediment transport. *Nature Communications*, 10(1), 4903. https://doi.org/10.1038/s41467-019-12753-x.

Beerbower, J.R., 1964. Cyclothems and cyclic depositional mechanisms in alluvial plain sedimentation. *Kansas Geological Survey, Bulletin*, 169(1), 31—42.

Burpee, A.P., Slingerland, R.L., Edmonds, D.A., Parsons, D., Best, J., Cederberg, J.A., McGuffin, A., Caldwell, R., Nijhuis, A., Royce, J., 2015. Grain-size controls on the morphology and internal geometry of river-dominated deltas. *Journal of Sedimentary Research*, 85(6), 699—714. https://doi.org/10.2110/jsr.2015.39.

Caldwell, R.L., Edmonds, D.A., 2014. The effects of sediment properties on deltaic processes and morphologies: A numerical modeling study. *Journal of Geophysical Research: Earth Surface*, 119(5), 961—982. https://doi.org/10.1002/2013JF002965.

Cecil, C.B., 2003. The concept of autocyclic and allocyclic controls on sedimentation and stratigraphy, emphasizing the climatic variable. In: Cecil, C.B., Edgar, T.N. (Eds.), *Climate Controls on Stratigraphy*, vol. 77. SEPM Special Publication, pp. 13—20.

Chadwick, A.J., Steele, S., Silvestre, J., Lamb, M.P., 2022. Effect of sea-level change on river avulsions and stratigraphy for an experimental lowland delta. *Journal of Geophysical Research: Earth Surface*, 127(7). https://doi.org/10.1029/2021JF006422 e2021JF006422.

Donaldson, A.C., 1966. Deltaic sands and sandstones. *Symposium on Recently Developed Geologic Principles and Sedimentation of the Permo-Pennsylvanian of the Rocky Mountains; 20th Annual Conference*, pp. 31—62.

Edmonds, D.A., Hoyal, D.C.J.D., Sheets, B.A., Slingerland, R.L., 2009. Predicting delta avulsions: Implications for coastal wetland restoration. *Geology*, 37(8), 759—762.

Edmonds, D.A., Slingerland, R.L., 2007. Mechanics of river mouth bar formation: Implications for the morphodynamics of delta distributary networks. *Journal of Geophysical Research: Earth Surface*, 112(F2), F02034. https://doi.org/10.1029/2006JF000574.

Feng, W.J., Lu, F.M., Wu, S.H., Zhang, Y., Meng, Q.L., Zhang, K., 2018. Reservoir architecture analysis of braided delta front developed in the long-axis gentle slope of faulted basin: A case study of the fifth Zaoyuan Formation, Zaonan fault block, Zaoyuan Oilfield, Dagang. *Journal of China University of Mining & Technology*, 47(2), 367—379 (in Chinese with English abstract).

Frazier, D.E., 1967. Recent deltaic deposits of the Mississippi River: Their development and chronology. *Transactions - Gulf Coast Association of Geological Societies*, 17, 287—315.

Fu, J., Wu, S.H., Wang, Z., Liu, Y.M., 2015. Architecture model of shallow-water delta distributary channel in lake basin: A case study of the Yanchang Formation outcrops in the eastern margin of Ordos Basin. *Journal of*

Central South University, 46(11), 4174—4182 (in Chinese with English abstract).

Ganti, V., Chadwick, A.J., Hassenruck-Gudipati, H.J., Lamb, M.P., 2016. Avulsion cycles and their stratigraphic signature on an experimental backwater-controlled delta. *Journal of Geophysical Research: Earth Surface*, 121(9), 1651—1675. https://doi.org/10.1002/2016JF003915.

Ganti, V., Chu, Z.X., Lamb, M.P., Nittrouer, J.A., Parker, G., 2014. Testing morphodynamic controls on the location and frequency of river avulsions on fans versus deltas: Huanghe (Yellow River), China. *Geophysical Research Letters*, 41(22), 7882—7890. https://doi.org/10.1002/2014GL061918.

Gao, S., 2007. Modeling the growth limit of the Changjiang Delta. *Geomorphology*, 85(3), 225—236. https://doi.org/10.1016/j.geomorph.2006.03.021.

Hajek, E.A., Straub, K.M., 2017. Autogenic sedimentation in clastic stratigraphy. *Annual Review of Earth and Planetary Sciences*, 45, 681—709. https://doi.org/10.1146/annurev-earth-063016-015935.

Hamilton, L.C., Stampone, M.D., 2013. Blowin' in the wind: Short-term weather and belief in anthropogenic climate change. *Weather, Climate, and Society*, 5(2), 112—119. https://doi.org/10.1175/wcas-d-12-00048.1.

Holbrook, J.M., Willis, B.J., Bhattacharya, J., 2003. *The evolution of allocyclicity and autocyclicity as sedimentary concepts. AAPG Annual Meeting* (Salt Lake City, Utah).

Hoyal, D.C.J.D., Sheets, B.A., 2009. Morphodynamic evolution of experimental cohesive deltas. *Journal of Geophysical Research*, 114(F2), F02009. https://doi.org/10.1029/2007JF000882.

Ikeda, S., 1982. Lateral bed load transport on side slopes. *Journal of the Hydraulics Division*, 108, 1369—1373. https://doi.org/10.1061/JYCEAJ.0005937.

Liang, M., Van Dyk, C., Passalacqua, P., 2016. Quantifying the patterns and dynamics of river deltas under conditions of steady forcing and relative sea level rise. *Journal of Geophysical Research: Earth Surface*, 121(2), 465—496. https://doi.org/10.1002/2015JF003653.

Ma, R.H., Duan, H.T., Hu, C.M., Feng, X.Z., Li, A.N., Ju, W.M., Jiang, J.H., Yang, G.S., 2010. A half-century of changes in China's lakes: Global warming or human influence? *Geophysical Research Letters*, 37(24), L24106. https://doi.org/10.1029/2010GL045514.

Martin, J., Sheets, B., Paola, C., Hoyal, D., 2009. Influence of steady base-level rise on channel mobility, shoreline migration, and scaling properties of a cohesive experimental delta. *Journal of Geophysical Research*, 114(F3), F03017. https://doi.org/10.1029/2008JF001142.

Mishra, R.K., Dubey, S.C., Nagaraja, K., 2014. The role of sun on climate change. *Journal of Engineering Science*, 1, 8—14.

Moodie, A.J., Nittrouer, J.A., Ma, H., Carlson, B.N., Chadwick, A.J., Lamb, M.P., Parker, G., 2019. Modeling deltaic lobe-building cycles and channel avulsions for the Yellow River delta, China. *Journal of Geophysical Research: Earth Surface*, 124(11), 2438—2462. https://doi.org/10.1029/2019JF005220.

Muto, T., Steel, R.J., 2004. Autogenic response of fluvial deltas to steady sea-level fall: Implications from flume-tank experiments. *Geology*, 32(5), 401—404. https://doi.org/10.1130/G20296.1.

Nijhuis, A.G., Edmonds, D.A., Caldwell, R.L., Cederberg, J.A., Slingerland, R.L., Best, J.L., Parsons, D.R., Robinson, R.A.J., 2015. Fluvio-deltaic avulsions during relative sea-level fall. *Geology*, 43(8), 719—722. https://doi.org/10.1130/G36788.1.

Olariu, C., 2014. Autogenic process change in modern deltas: Lessons for the ancient. *IAS Special Publications*, 46, 149—166.

Stenchikov, G., 2021. The role of volcanic activity in climate and global changes. In: Letcher, T.M. (Ed.), *Climate Change*, third ed. Elsevier, Amsterdam, pp. 607—643. https://doi.org/10.1016/B978-0-12-821575-3.00029-3.

Straub, K.M., Li, Q., Benson, W.M., 2015. Influence of sediment cohesion on deltaic shoreline dynamics and bulk sediment retention: A laboratory study. *Geophysical Research Letters*, 42(22), 9808—9815. https://doi.org/10.1002/2015GL066131.

Van Rijn, L.C., 1993. *Principles of Sediment Transport in Rivers, Estuaries and Coastal Seas*. Aqua Publications, Amsterdam.

Wang, Y.W., Yu, Q., Jiao, J., Tonnon, P.K., Wang, Z.B., Gao, S., 2016. Coupling bedform roughness and sediment grain-size sorting in modelling of tidal inlet incision. *Marine Geology*, 381, 128—141. https://doi.org/10.1016/j.margeo.2016.09.004.

Wei, X., Cai, S.Q., Ni, P.T., Zhan, W.K., 2020. Impacts of climate change and human activities on the water discharge and sediment load of the Pearl River, southern China. *Scientific Reports*, 10(1), 16743. https://doi.org/10.1038/s41598-020-73939-8.

Wolinsky, M.A., Edmonds, D.A., Martin, J., Paola, C., 2010. Delta allometry: Growth laws for river deltas. *Geophysical Research Letters*, 37(21), L21403. https://doi.org/10.1029/2010GL044592.

Xu, Z.H., Wu, S.H., Wang, Q.L., Zhang, P., Deng, M., Feng, W.J., Zhang, J.J., Zhang, C.M., 2023. Internal architectural patterns of bar fingers within digitate shallow-water delta: Insights from the shallow core, GPR and Delft3D simulation data of the Ganjiang Delta, China. *Lithosphere*, 2022(Special 13), 9120724. https://doi.org/10.2113/2022/9120724.

Yin, S.L., Chen, G.Y., Dai, C.M., Wu, S.H., Lu, F.M., Feng, W.J., 2015. Reservoir architecture and remaining oil distribution in mouth bar—A case study on the braided delta of long-axis gentle slope in Zaonan fault block of Dagang Oilfield. *Oil & Gas Geology*, 36(4), 630—639. https://doi.org/10.11743/ogg20150413 (in Chinese with English abstract).

Yin, T.J., Zhang, C.M., Zhu, Y.J., Yang, W., Ye, J.G., Cai, W., Dai, Y.Y., 2014. Overlapping delta: A New special type of delta formed by overlapped lobes. *Acta Geologica Sinica*, 88(2), 263—272 (in Chinese with English abstract).